Motional Stark Effect Polarimetry for the Determination of the ASDEX Upgrade Current Density Profile

R. C. Wolf, P. J. Mc Carthy*, F. Mast, H.-P. Zehrfeld, and the ASDEX Upgrade Team

Max-Planck-Institut für Plasmaphysik, EURATOM
Association, D-85748 Garching, Germany
*University College Cork, Association EURATOM-DCU, Cork Ireland

1. Introduction. For the analysis of transport and stability of tokamak plasmas accurate knowledge of the current density profile and related quantities, such as safety factor and magnetic shear, is required. Motional Stark effect (MSE) polarimetry, which measures the internal local poloidal magnetic field, has become one of the most important methods for the determination of the current density [1, 2, 3]. At ASDEX Upgrade a 10-channel MSE polarimeter, using the modulation technique [4] and observing one of the 2.5MW, 65keV heating beams is under development.

2. Outline of diagnostic. The observation geometry crucially influences the performance of the polarization measurement. At ASDEX Upgrade the choice was to use one of four existing heating beams and to select one of 16 observation ports located every 22.5° between the toroidal field coils. As the heating beams are inclined at 4.9° to the midplane of the torus, a horizontal observation geometry could not be realized. For a selected, the three parameters pitch angle projection factor, spatial resolution, and spectral separation of full and half energy fractions have to be optimized simultaneously. An outline of the diagnostic with a planar view of the chosen observation geometry is shown in fig. 1. The resulting pitch angle projection factor, given by tan(polarization angle)/tan(pitch angle), ranges from 0.40 at the plasma centre to 0.75 at the plasma edge. The spatial resolution, determined by the angle between the viewing line and magnetic field, where the neutral beam volume intersects the viewing line, drops from 6cm at the plasma centre to 2cm at ρ=0.3 and rises again to 9cm at the plasma edge. The observation optics consists of a dielectric mirror followed by four lenses, which for each of the ten spatial channels images the neutral beam onto six vertically stacked 1mm diameter optical fibres. With a demagnification of 20 this corresponds to a 2cm wide and 12cm high spot in the plasma covering about 2/3 of the FWHM of the beam. The lens system exhibits an étendue of $\Omega A = 2.4 \times 10^{-6}$sr m^2 corresponding to f/1.4 at the fibre side, which is still below the theoretical limit of the fibres of f/1.

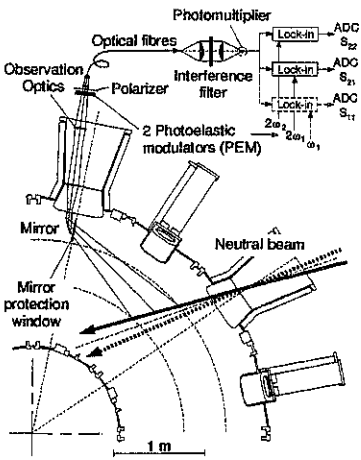

Fig. 1.: Outline of MSE diagnostic. The polarimeter design is similar to that described in [5].

3. Spectral simulation. A spectral simulation for the given geometry, taking beam and viewing line divergence as the main line broadening mechanisms, is shown in fig. 2. The

σ-component of the full energy fraction, which is to be used for the polarization measurement, is well separated from the π-component of the half energy fraction, which is the prime condition for a large polarization fraction at the σ-wavelength. In addition, the σ-component of the neutral beam used for MSE is, for all radii, sufficiently separated from the Stark spectrum of the other beam intersected by the viewing lines, to allow all heating beams to be operated simultaneously during MSE measurements. The optimum FWHM of the interference filters, derived from the spectral simulation, lies between 0.2 and 0.3nm depending on magnetic field and beam energy.

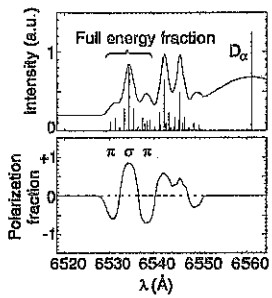

Fig. 2.: Spectral simulation of Doppler shifted Balmer-α beam emission spectrum and corresponding polarization fraction at ρ=0.3 for a 60keV deuterium beam, B_{tor}=2T, and T_i=3keV.

4. Faraday rotation. Faraday rotation in the MSE polarimeter, induced by the tokamak magnetic field, causes an offset in the polarization measurement. As suggested in [5], the use of Schott SFL6 glass with a Verdet constant of zero reduces the Faraday rotation significantly. For components not made of SFL6, such as the vacuum window or PEMs, a half wave plate positioned between the optical elements, so that the Faraday rotation angles before and after the half wave plate are equal, eliminates the net Faraday rotation. The condition of equal Faraday rotation angles means that in an inhomogeneous magnetic field B(x) using materials with different Verdet constants V(x) the integral along the optical axis $\int B(x)V(x)dx$ has to be the same before and after the half wave plate.

5. Influence of mirror. The use of a mirror is required, because a tangential access for the beam observation is not available. The polarization properties of the mirror, however, introduce a systematic error into the angle measurement (fig. 3). Here, the systematic error is the difference between the actual angle and that derived from the polarimeter signals. Two cases are distinguished in Fig. 3: (1) The apparent angle is deduced only from the ratio of the intensity modulation amplitudes at twice the PEM frequencies (dashed lines) and (2) in addition the phase shift is reconstructed from the modulation amplitude at the single PEM frequency (solid lines). It can be seen that for a horizontal viewing geometry, where the polarization angle of the σ-component is close to the mirror p-polarization, the systematic error approaches zero. At ASDEX Upgrade, however, due to the non-horizontal viewing geometry the polarization angle lies in the vicinity of 67° (shaded area), which requires corrections to the phase shift in order to minimize the systematic error.

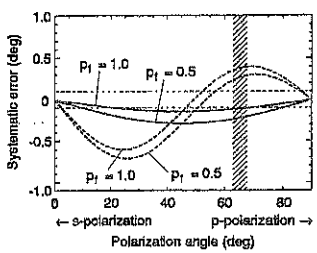

Fig. 3.: Systematic error introduced by a mirror (ρ_p=0.995, δ_p−δ_s=15°) as a function of polarization angle. The systematic error increases with decreasing polarization fraction p_f.

6. Current profile identification using MSE. To quantify the expected improvement in determining $j(R,z)$ with MSE measurements, a sensitivity study has been carried out using

a database of 1100 ideal MHD equilibria with 21 degrees of freedom, including I_p, B_t, 10 active and 2 passive poloidal field coil currents, and (with I_p scaled out) a 7-parameter $j_t = Rp'(\psi) + FF'(\psi)/(\mu_o R)$ profile family given by (with $\hat{\psi}$ the normalized poloidal flux)

$$p'(\hat{\psi}) \propto \hat{\psi}^{a_P} \exp\left\{b_P(1-\hat{\psi}) + c_P(1-\hat{\psi})^2\right\}$$

where a_P, b_P, c_P are randomly chosen for each $p'(\hat{\psi})$ profile, a_{FF}, b_{FF}, c_{FF} specify the $FF'(\hat{\psi})$ profile, and the 7th parameter determines β_{pol}. Reversed shear and edge pedestal profiles are easily generated with this family, and the wide range of current profiles in the database satisfies $0.5 < I_p < 2$MA, $1 < B_t < 4$T, $0 < \beta_{pol} < 2$, $0.5 < l_i < 2$, $0.5 < q_o < 4$, $2 < q_{95} < 6$, and reversed shear characterized by $1 \leq q_o/q_{min} < 4$.

6.1. Database Details. For each equilibrium in the database, all diagnostic data required for the study are calculated using the correct experimental geometry. These include 36 magnetic flux and field probes and 10 MSE channels. To gauge the usefulness of the MSE diagnostic compared to its main alternative, namely Faraday Rotation (FR) polarimetry (not to be confused with the nuisance effect of FR on the MSE measurements as outlined earlier), a hypothetical FR diagnostic on ASDEX Upgrade using the geometry of the 8-channel DCN (195 μm) interferometer is also simulated. For this purpose, a randomly generated $n_e(\psi)$ profile, chosen from a 5-parameter family, is assigned to each equilibrium and the differential equation describing the change in polarization along the beam path is integrated numerically so that Cotton Mouton effects are fully accounted for in the simulated FR measurements. Both MSE and FR geometries are shown in Fig. 4 and for the present database these yield angles with typical magnitudes of 5° for MSE and 8° for FR.

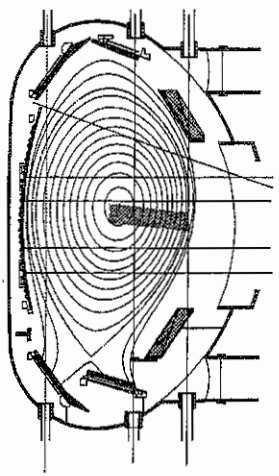

Fig. 4.: ASDEX Upgrade equilibrium flux surfaces. Shaded box near mid-plane indicates area spanned by 10 MSE channels. Geometry of 8 DCN channels is shown by straight lines criss-crossing the flux surfaces.

6.2. Identification Algorithm Starting from a baseline set of 36 equilibrium magnetic measurements and B_t, $j(R,z)$ identification representative of the entire database is monitored as MSE channels are progressively added to the baseline set. This is accomplished using the method of Function Parameterization [6] where here the current profile is regressed as a second degree polynomial whose arguments are B_t+16 principal components of the external magnetic measurements augmented by the MSE data. For the FR study, the MSE channels are replaced by the FR data consisting of two signals per channel, namely the line-integrated electron density and the rotation angle. The root mean squared errors (rmse) from the regressions are a measure of the recoverability of the current profile. For MSE, the finite spatial resolution of the viewing geometry (the horizontal resolution varies between 2 and 8 cm; the vertical resolution is 12 cm) is taken into account. For both MSE and FR, simulated measurement noise chosen from a uniform distribution in the range $\pm d°$ is added to the

"measured" angles. A sequence of runs was made with different values of d to determine the degradation of the recovery with increasing d.

6.3. Results. Fig. 5 shows 2×rmse, i.e. ≈ 95% confidence bands for $j(r,z)$ (where $r = (R-R_o)/a$ is a purely geometric quantity) identification along the $z = z_{mag.axis}$ plane (which spanned the range $0 \leq z_{mag.axis} \leq 0.2\,\mathrm{m}$ in the database) where both sets of data were perturbed by the experimentally expected noise level of ±0.2°. To facilitate the MSE/FR comparison, the outer two MSE channels were not used in this analysis. There is little to distinguish MSE and FR in the range $.5 < |r| < 1$. Near the plasma centre, however, the MSE identification is clearly better. For $j(r=0, z_{mag})$, the error reduction factor with respect to the baseline model is 4.2 for MSE, 3.1 for FR. The corresponding factors for $j(r=0.9, z_{mag})$ are 1.7 and 1.55. The localized nature of MSE may explain its superiority over FR at the plasma centre. Fig. 6 shows the effect of noise on the rms regression errors for the reversed shear indicator q_o/q_{min}. The rmse is trended for the cases of 3, 6 and all (9 for MSE, 8 for FR) channels included in the regressions (the point at infinity corresponds to the magnetics-only regression). As expected from their typical magnitudes (see 6.1.), the MSE measurements are more sensitive to noise than FR, although at a level of ±0.2° MSE is much more accurate than FR. Note the FR errors tend to reach a plateau. This was found to be due to the topological information present in the $\int n_e\, dl$ measurements, which were unperturbed by noise.

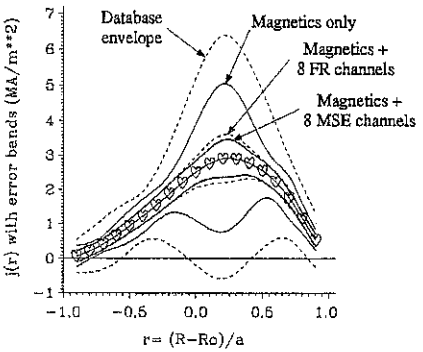

Fig. 5.: Mean $j(r, z_{mag})$ profile in the equilibrium database (♡) surrounded by (i) 2 × Std.Dev. envelope indicating the variation over the database of $j(r, z_{mag})$ about its mean, (ii) 2 × rmse confidence bands for the baseline (magnetics-only) regression, (iii) for the baseline set + all 8 FR channels, and (iv) for the baseline set + MSE channels 1-8, where noise of magnitude ±0.2° was added to both FR and MSE data.

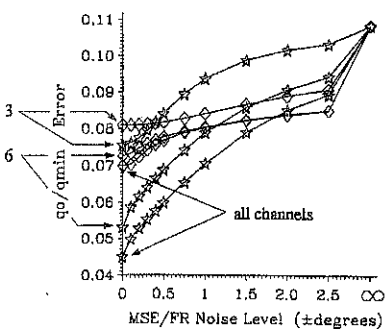

Fig. 6.: rmse for the parameter q_o/q_{min} versus error in the measured angle for MSE (⋆) and FR (◇) regressions with 3, 6, and all channels added to the Magnetics-only model.

6.4. Summary. Provided the experimental variation in $j(r,z)$ is described by the profile family used here, MSE is expected to reduce the uncertainty in $j(r,z)$ relative to a magnetics-only identification by a factor of ≈ 4 at the plasma centre and ≈ 1.5 near the edge.

7. References

[1] S. H. Batha et al., Nucl. Fusion 36, 1133 (1996)
[2] B. W. Rice et al., Phys. Plasmas 3, 1983 (1996)
[3] R. C. Wolf et al., Nucl. Fusion Lett. 33, 663 (1993)
[4] F. M. Levinton et al., Phys. Rev. Lett. 63, 2060 (1989)
[5] B. W. Rice et al., Rev. Sci. Instrum. 66, 373 (1995)
[6] P. J. Mc Carthy, Ph.D. thesis, University College Cork (1992)